



Electrochemical Biosensor with Enhanced Antifouling Capability for COVID-19 Nucleic Acid Detection in Complex Biological Media

Zhen Song,[†] Yihui Ma,[†] Min Chen, Adriano Ambrosi, Caifeng Ding,^{*} and Xiliang Luo^{*}



Cite This: *Anal. Chem.* 2021, 93, 5963–5971



Read Online

ACCESS |



Metrics & More

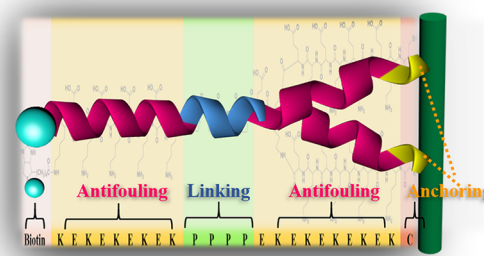


Article Recommendations



Supporting Information

ABSTRACT: Biofouling caused by the accumulation of biomolecules on sensing surfaces is one of the major problems and challenges to realize the practical application of electrochemical biosensors, and an effective way to counter this problem is the construction of antifouling biosensors. Herein, an antifouling electrochemical biosensor was constructed based on electro-polymerized polyaniline (PANI) nanowires and newly designed peptides for the detection of the COVID-19 N-gene. The inverted Y-shaped peptides were designed with excellent antifouling properties and two anchoring branches, and their antifouling performances against proteins and complex biological media were investigated using different approaches. Based on the biotin–streptavidin affinity system, biotin-labeled probes specific to the N-gene (nucleocapsid phosphoprotein) of COVID-19 were immobilized onto the peptide-coated PANI nanowires, forming a highly sensitive and antifouling electrochemical sensing interface for the detection of COVID-19 nucleic acid. The antifouling genosensor demonstrated a wide linear range (10^{-14} to 10^{-9} M) and an exceptional low detection limit (3.5 fM). The remarkable performance of the genosensor derives from the high peak current of PANI, which is chosen as the sensing signal, and the extraordinary antifouling properties of designed peptides, which guarantee accurate detection in complex systems. These crucial features represent essential elements for future rapid and decentralized clinical testing.



Coronavirus disease 2019 (COVID-19), caused by the 2019 novel coronavirus (2019-nCoV), is a new severe respiratory disease accompanied by fever, breathlessness, and cough. Following the first discovery in December 2019, it rapidly swept around the world and was classified as a pandemic by the World Health Organization (WHO) on March 12, 2020.¹ According to the report from the WHO, over 105.3 million cases and 2.3 million deaths have been confirmed globally as of Feb 8, 2021.² Unfortunately, no medical treatment is yet available to specifically cure COVID-19 disease or prevent the viral infection, and with exponential diffusion still experienced by several countries in the world, social distancing, personal hygiene habits, and more importantly an accurate and massive screening of the population, for early diagnosis of the disease, represent the currently available weapons to best fight the pandemic.

At present, reverse-transcription polymerase chain reaction (RT-PCR), which is widely available for clinical samples, such as nasal and pharyngeal swabs, blood, excrement, and so on, is referred to as the “gold standard” techniques.^{3–5} However, high demand for kits, tedious sample collection, and transportation become the major limitations. Next, a lateral flow immunoassay can realize rapid and real-time detection with a sample device, but it cannot diagnose the positive cases in its early stage due to the fact that detectable antibodies are produced by the body only after several weeks from the

infection.⁶ In addition, chest computed tomography (CT) is considered as the most effective means of disease diagnosis, but it is only available in hospitals and clinics and due to its high costs and limited availability cannot be employed for rapid and massive testing.^{7,8} Hence, development of a time-saving, highly sensitive and accurate, cost-effective method for COVID-19 detection is urgently needed and would have a significant impact for dealing with this pandemic.

Compared with the currently existing diagnostic approaches, electrochemical biosensors possess important characteristics that perfectly fit the current requirements, such as ease of operation, cost effectiveness, portable equipment, rapidity and high sensitivity.^{9,10} However, interface biofouling arising from the biomolecule adsorption represents one of the major problems for electrochemical sensing platforms and restricts their practical application.^{11,12} One possible solution to this problem is the creation of a sensing interface modified with an effective antifouling film, which limits non-specific adsorption

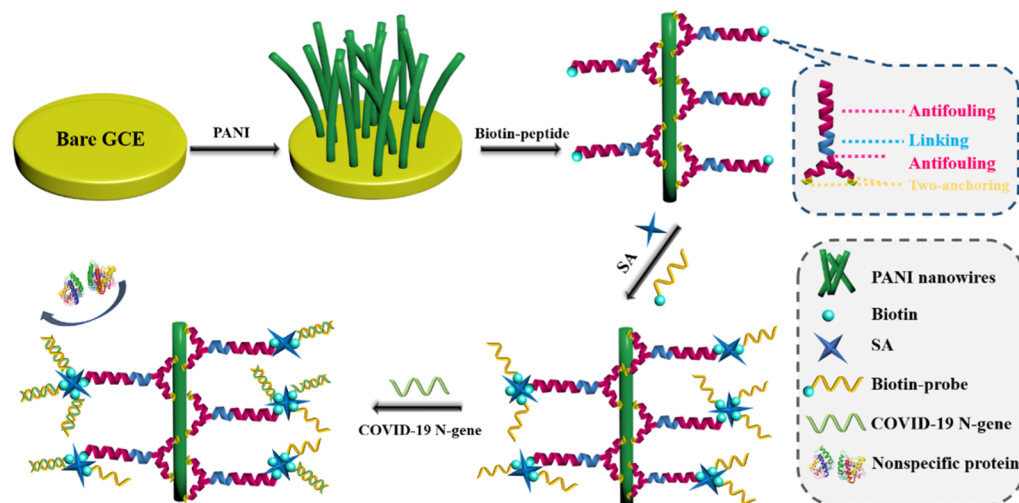
Received: February 17, 2021

Accepted: March 23, 2021

Published: April 2, 2021



Scheme 1. Schematic Diagram of the Antifouling COVID-19 Genosensor Fabrication Process



of biomolecules without interfering with the specific analyte recognition and detection. In addition, such an antifouling material introduced should be biocompatible and non-toxic, so that it can be used even in wearable or implantable devices.¹³ Peptides represent excellent candidates as antifouling agents due to their good biocompatibility and biodegradability. Several peptides with different structure designs and sequences have been applied as antifouling films.^{9,11,14,15} For example, Nowinski and co-workers designed a zwitterionic peptide (CPPPPEKEKEKE) with an alternating arrangement of glutamic acid (E, negatively charged) and lysine (K, positively charged), which is similar to zwitterionic polymers,¹⁶ that can form a hydrated layer, effectively resisting biofouling ($<0.3 \text{ ng} \cdot \text{cm}^{-2}$).¹⁷ Two short sequences PFB-VVD and PFB-LLE (PFB: pentafluorobenzaldehyde) with chemical modification have also shown good ability to resist protein adsorption.¹⁸ In another work, a branched zwitterionic peptide (CPPPPEK2-(EK)4(EK)) designed by Liu and co-workers demonstrated superior resistance to human serum and cell adhesion over linear sequences.¹⁹

Due to its fast and reversible doping/de-doping kinetics, multiple redox states, high conductivity, and cost-effective synthesis, polyaniline (PANI) has been widely used in fabrication of sensing interfaces.^{20–22} More importantly, the structure of PANI can be easily tuned by simply changing the parameters during the electrochemical deposition, achieving excellent control over its resulting structure. Besides, the availability of abundant amino groups provides an ideal platform for further grafting biomolecules.

In this work, we fabricate electrically polymerized PANI nanowires as the electrode coating for the immobilization of a newly designed inverted Y-shaped peptide as an antifouling agent and the specific N-gene capture probe (an antisense oligonucleotide) as a recognition element for the detection of the COVID-19 N-gene (nucleocapsid phosphoprotein gene) (Scheme 1). The newly designed inverted Y-shaped peptide ((CKEKEKEKE)₂KEPPPPKEKEKEKEK-biotin) consists of one antifouling main chain (KEPPPPKEKEKEKEK-biotin) in the upper part, which has four proline residues (PPPP) assisting in the formation of the α -helical secondary structure, and two anchor-antifouling side chains (CKEKEKEKE) in the lower part. Two cysteine (C) residues at the ends of the two side chains were used as the surface anchor to immobilize the

peptides onto the PANI nanowires through the sulfo-SMCC cross-linking. The presence of two anchor chains guarantees a robust and stable immobilization onto the electrode while providing enhanced flexibility of the main chain where the probe is attached. Such an innovative design contributes to high interface coverage and a better antifouling performance compared with the standard single anchor design.^{19,23} Thereafter, streptavidin (SA, a tetramer protein) was employed as a linker to immobilize the N-gene capture probe on biotin-peptide-covered interfaces based on the biotin-streptavidin affinity system. The sensing platforms based on the biotin-streptavidin interaction, proved to be an effective way of constructing biosensors, have been widely reported.^{24–27} The biotin-labeled branched peptides were first conjugated with SA, which provides four specific binding sites for the immobilization of the biotin-labeled N-gene probe. A SA-biotin immobilization scheme was employed since the zwitterionic property of the peptide can be significantly affected by the covalent immobilization of the probe through amide bonds.^{11,28} The resulting electrochemical genosensor for COVID-19 N-gene detection was tested with complex serum samples, demonstrating excellent detection limit and specificity thanks to the improved antifouling properties.

EXPERIMENTAL SECTION

Reagents. A newly designed inverted Y-shaped peptide labeled with biotin ((CKEKEKEKE)₂KEPPPPKEKEKEKEK-biotin) and a linear peptide labeled with biotin (CKEKEKEKEKEPPPPKEKEKEKEK-biotin) as the control group used in this work were designed by us and synthesized by Bank-peptide Biological Technology Co. Ltd. (Hefei, China). The N-gene probe labeled with biotin (antisense oligonucleotide: 5'-biotin-CCAATGTGATCTTTTGGTGT-3'), target sequence (N-Gene of Covid-19: 5'-ACACCAAAAGAUCACAUUGG-3'), noncomplementary sequence (5'-UUCUUC-GAACGU GUCACGU-3'), Cy5-DNA (TCAACAT-CAGTCTGATAAGCTA), miRNA-141, miRNA-21, FITC-BSA, and SA were provided by Sangon Biotech Co., Ltd. (Shanghai, China) and stored at $-20 \text{ }^\circ\text{C}$. 4-(N-Maleimidomethyl)-cyclohexane-1-carboxylic acid 3-sulfo-N-hydroxysuccinimide ester sodium salt (sulfo-SMCC) was ordered from Sigma-Aldrich (USA). Perchloric acid (HClO_4) and aniline were provided by Aladdin Reagents (Shanghai, China).

Myoglobin (Mb), albumin (BSA), lysozyme (Lys), and fetal bovine serum (FBS) were ordered from Beijing Bo Yang Hongda Technology Co., Ltd. (Beijing, China). The Eighth People's Hospital of Qingdao provided the human serum samples from volunteers for us, and advanced informed agreement was obtained for the use of the human serum. All samples were prepared under the authority of the committee of the Eighth People's Hospital of Qingdao and conducted in accordance with the relevant guidelines and laws. All chemicals were of analytical grade. During the entire process of the experiment, the ultrapure water ($18 \text{ M}\Omega\text{-cm}^{-1}$) was purified using a Milli-Q water system (USA) and applied for preparing aqueous solutions. The working buffer was 10 mM and 0.2 M phosphate-buffered solution (PBS, pH 7.4).

Apparatus and Measurements. All electrochemistry measurements were carried out using a CHI 660E electrochemical workstation (Shanghai Chenhua Instrument Co., China). Electrochemical testing was performed using a three-electrode system: reference electrode (a saturated calomel electrode, SCE), counter electrode (a platinum wire), and working electrode (a bare or modified glassy carbon electrode, GCE, 3.0 mm in diameter). A galvanostatic technique was used for modification of the GCE with PANI nanowires. Electrochemical performance of the biosensor was recorded by differential pulse voltammetry (DPV) and cyclic voltammetry (CV). DPV and CV were measured within a detection voltage from -0.6 to 0.6 V at a scan rate of $100 \text{ mV}\cdot\text{s}^{-1}$ and an amplitude of 50 mV in phosphate-buffered saline (PBS, 0.2 M, pH 7.4).

The surface characterizations of the modified electrodes were carried out by means of a JEOL JSM-7500F scanning electron microscope (SEM, Hitachi Co., Japan). The fluorescence images of the antifouling performance were conducted with a TCS SP5 confocal laser microscope (Leica, Germany). Fourier transform infrared spectroscopy (FTIR) was used to characterize the elemental changes of the modified electrodes using the Bruker Tensor 70 spectrometer. X-ray photoelectron spectroscopy (XPS) spectra were recorded with an ESCALAB 250Xi spectrometry (Thermo Fisher Scientific, U.K.) instrument with a monochromatic Al $K\alpha$ X-ray source ($h\nu = 15 \text{ kV}$); all spectra were calibrated to the standard value of the C(1s) peak (284.6 eV). A Zetasizer Nano-ZS (Malvern Instruments, Malvern, U.K.) and software calculation were used to measure the net charge of the peptides. The secondary structure of the peptides was verified using a JASCO J-810 spectropolarimeter (Jasco Inc., Japan) and the corresponding circular dichroism (CD) spectra. A JC2000D1 system (Shanghai Zhongchen, China) was employed to evaluate the hydrophilic properties of the modified or bare GCE.

Synthesis of PANI Nanowires and Preparation of the Antifouling Interface. Prior to assembly, the bare GCE was polished²⁹ and then treated in an ultrasonic bath with water, ethanol, and water. The pretreated bare GCE was immersed in 0.1 M PANI diluted with 1.0 M HClO_4 , and PANI nanowires were electrodeposited on it using a galvanostatic technique. PANI electrodeposition was conducted with three constant current densities of 0.6, 0.3, and $0.15 \text{ mA}\cdot\text{cm}^{-2}$ for 0.5, 0.5, and 0.5 h in sequence, respectively. Abundant amino groups in PANI provided the conditions for immobilization of peptides. The obtained PANI nanowire-modified GCE (PANI/GCE) was washed with deionized water, and then, PANI/GCE was pretreated with 2 mM sulfo-SMCC solution for 1 h before attaching the peptides. The modified electrodes were then

incubated in a solution containing $2.0 \text{ mg}\cdot\text{mL}^{-1}$ biotin peptides in phosphate-buffered saline (PBS, 0.2 M, pH 7.4) for 3 h. As a result, the antifouling interface (biotin-peptide/PANI/GCE) was obtained.

Immobilization of the Covid-19 N-Gene Probe. Here, binding of the biotin probe to the biotin peptides depended mainly on the specific interaction between biotin and SA. According to previous studies,^{30,31} the designed peptide-modified electrodes (biotin-peptide/PANI/GCE) were exposed to $2 \mu\text{M}$ SA solution for 1 h at 37°C . After washing, the abovementioned electrodes were incubated in $1 \mu\text{M}$ biotin probe solution at 37°C for 90 min. After further washing, the prepared biosensor was stored at 4°C before use.

Characterization of the Newly Designed Inverted Y-Shaped Peptide. CD spectrum was employed to obtain the secondary structure information of the newly designed inverted Y-shaped peptide in the wavelength range from 190 to 300 nm and a step resolution of 0.5 nm, using a $0.5 \text{ mg}\cdot\text{mL}^{-1}$ peptide suspension. Zeta potential measurements were used to evaluate the charges of the peptides. The hydrophilicity property of the peptide-modified surfaces was measured using the water contact angle.

Antifouling Performance and Fluorescence Imaging. The antifouling performance testing of the modified electrodes with or without designed inverted Y-shaped peptides was performed in a series of single-protein solutions (BSA, Lys, and Mb) and practical media (FBS and human serum solutions). Current changes were recorded by DPV measurements before and after incubation in interfering solutions. PBS buffer (10 mM, pH 7.4) was used to dilute the proteins and complex biological samples.

The fluorescence images of the modified electrodes were acquired after incubation in fluorescein isothiocyanate-labeled bovine serum albumin (FITC-BSA) and Cy5-labeled DNA (Cy5-DNA) solutions for 2 h. The bare GCE was selected as the control group. After thorough washing, the treated electrodes were placed into the imaging instrument. Then, the imaging system was used to image the biotin-peptide/PANI-modified electrodes, PANI film electrodes, and bare GCE individually (ex: $488 \text{ nm} \pm 10 \text{ nm}$, 10 s exposure).

Detection of the N Gene of Covid-19 (Target RNA). The biosensor was incubated in target N-gene solution with different concentrations at 37°C for 1 h. Afterward, non-captured target RNA was washed with PBS buffer and the abovementioned electrodes were prepared for electrochemistry detection. The changes in the current signal were recorded before and after specific binding with target RNA using an electrochemical station. To further evaluate the application potential in complex samples, the biosensor was used to analyze targets in 20% (V/V) human serum with all the other conditions unchanged.

RESULTS AND DISCUSSION

Characterization Studies of the Newly Designed Inverted Y-Shaped Peptide. The structure, chromatogram, and mass spectra of the newly designed inverted Y-shaped peptide are shown in Figures S1 and S2. The antifouling performance of the interfaces directly depends on the properties of used peptides. Biofouling processes are usually caused by charge and hydrophobic interactions between interferents and interfaces as demonstrated in the past.^{32,33} Hence, electrical and hydrophilic properties of the designed peptide were investigated. A peptide property calculator was

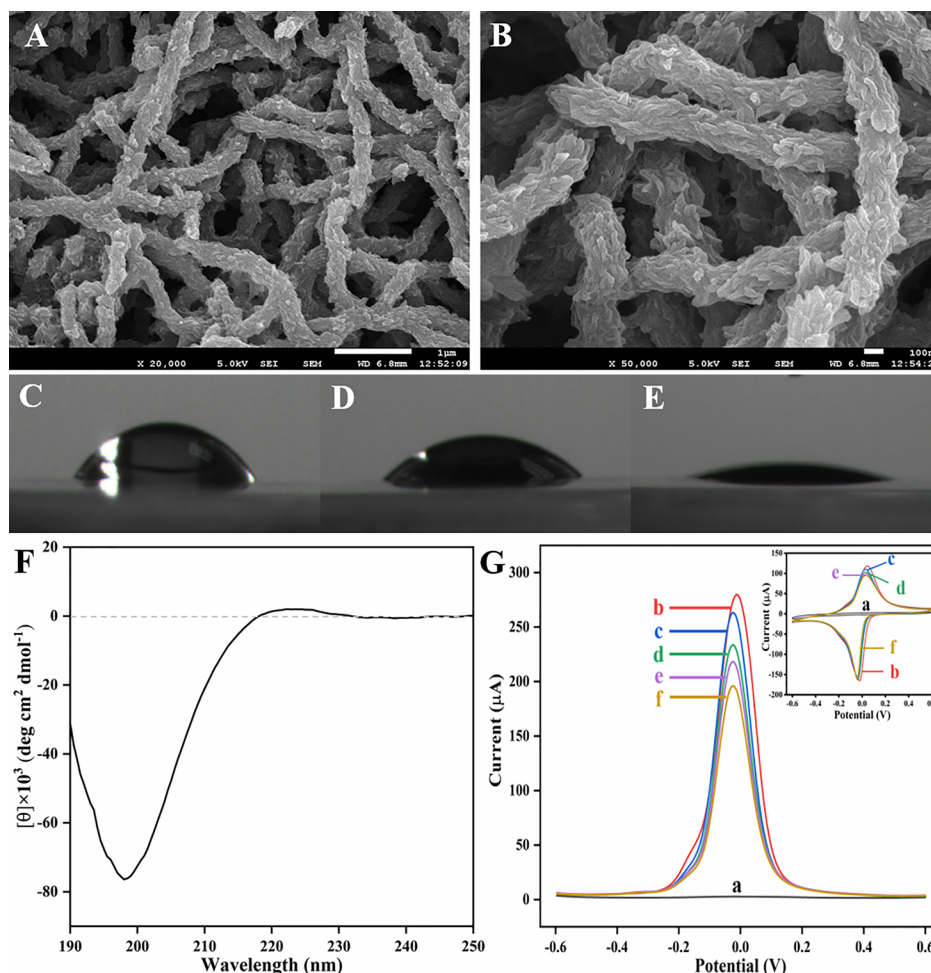


Figure 1. SEM images of the PANI nanowire film at low (A, ×20k) and high (B, ×50k) magnifications. Water contact angles of the bare GCE (C), PANI/GCE (D), and biotin-peptide/PANI/GCE (E). CD spectra (F) of the newly designed inverted Y-shaped peptide in PBS at a concentration of 0.5 mg·mL⁻¹. DPV response (G) of the bare GCE (a), PANI/GCE (b), biotin-peptide/PANI/GCE (c), SA/biotin-peptide/PANI/GCE (d), biotin-probe/SA/biotin-peptide/PANI/GCE (e), and target RNA/biotin-probe/SA/biotin-peptide/PANI/GCE (f) in PBS (0.2 M, pH 7.4).

used to quantify the net charge of the peptide at pH = 7. As depicted in Figure S3A,B, the non-labeled and biotin-labeled peptide sequence has positive 0.9 and negative 0.1 net charge, respectively. This illustrates that the charges of the designed peptide were effectively neutralized when the end lysine residue is combined with biotin. Next, the zeta potential of biotin-labeled peptide was close to 0.0 mV; see Figure S3C. These results suggested that the designed peptide was electrically neutral. Furthermore, it is worth noting that hydrophobicity and hydrophilicity are perhaps the most important gauge of the anti-contamination ability and play a crucial role in the design and selection of effective antifouling materials.^{13,18}

Hence, it is important to understand the interaction between water and the modified surface. As displayed in Figure 1C,D and Table S1, the water contact angle of the bare GCE and PANI/GCE was about 55.85° and 41.87°, respectively. After peptide immobilization, the water contact angle decreased from 41.87° (PANI/GCE) to 16.09° (biotin-peptide/PANI/GCE), indicating that the surfaces were more hydrophobic. This change can mainly stem from the good hydrophilicity of the newly designed inverted Y-shaped peptide (Figure 1E).

The secondary structure of the inverted Y shaped peptide was elucidated using CD spectra (Figure 1F). It is clear that a

weak positive band and a strong negative band appeared at 225 and 200 nm, respectively, portending the generation of the polyproline helix conformation of the Y-shaped peptide.^{17,34}

Characterization of the Surface Modification and Biosensor Assembly Process. The morphology of the PANI-coated GCE was characterized by SEM, as shown in Figure 1A,B. Interestingly, the PANI grown on the GCE formed a uniform nanowire network structure with the diameter of 150–200 nm, exhibiting a very high specific surface area.

The biosensor assembly process was monitored using electrochemical measurements. As shown in Figure 1G, current changes were recorded upon different modification steps in 0.2 M PBS solution (pH 7.4). Clearly, the DPV curve of the bare GCE presents no peak. Upon PANI nanowire deposition onto the GCE, an obvious current peak (curve b) was observed at the potential of -0.01 V, which is associated with the transition between leucoemeraldine and emeraldine conformations of the PANI polymer. After incubation with the biotin peptide (curve c), SA (curve d), and biotin probe (curve e), the current signal of the modified electrode further decreased. These results may be explained by the poor conductivity and space effect of the biomolecules, which could block the charge transfer between the interface and the solution. Finally, further

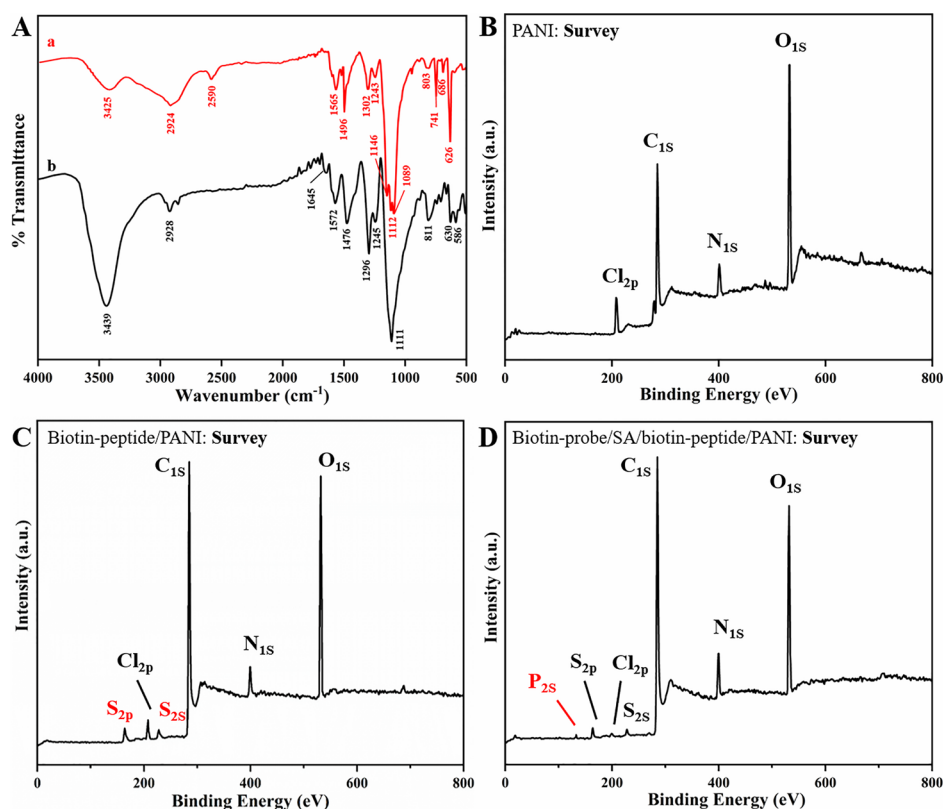


Figure 2. FTIR spectra (A) of PANI (a, red line) and biotin-peptide/PANI (b, black line). XPS survey scans of PANI (B), biotin-peptide/PANI (C), and biotin-probe/SA/biotin-peptide/PANI (D).

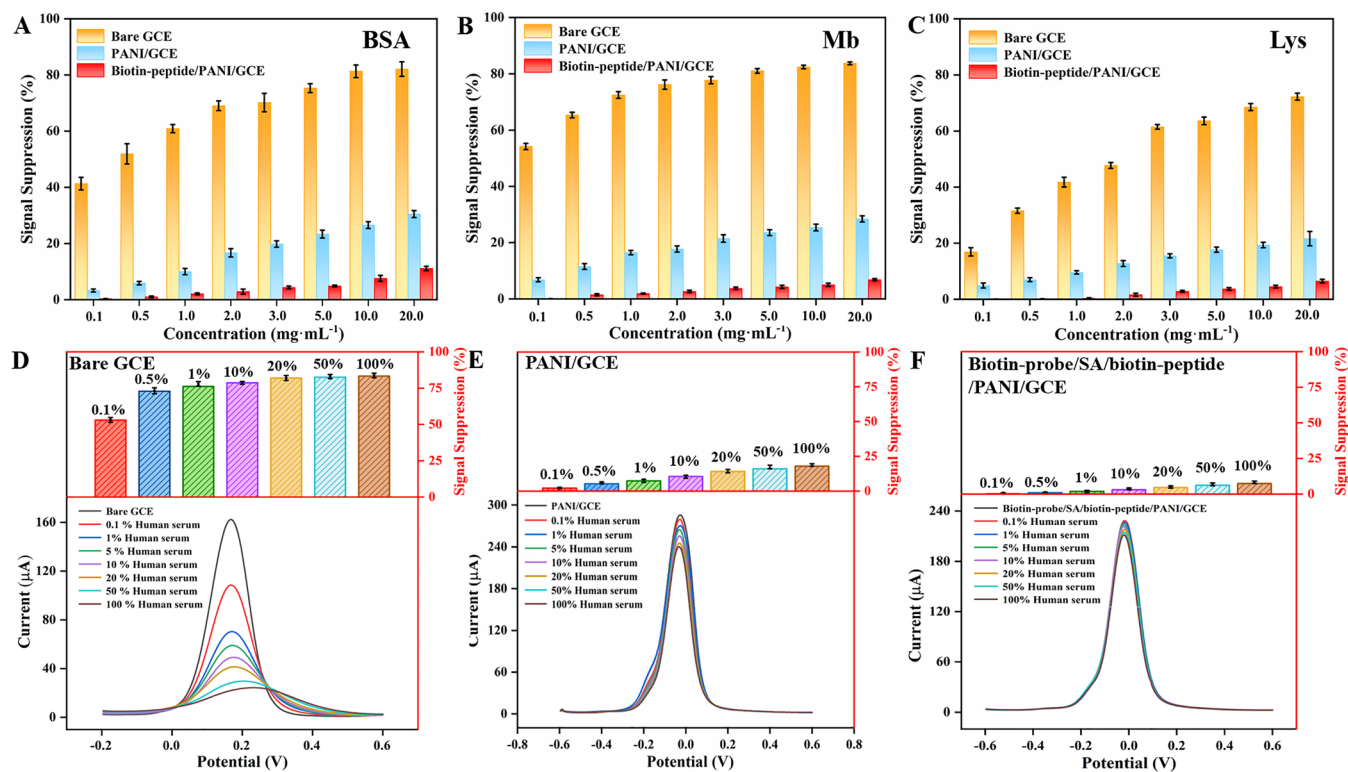


Figure 3. Histogram of antifouling performance of different modified surfaces against several single proteins (A: BSA, B: Mb, and C: Lys). Antifouling characteristics of the bare GCE (D), PANI/GCE (E), and biotin-probe/SA/biotin-peptide/PANI/GCE (F) in different concentrations of human serum samples (V/V). Lower parts are original DPV curves and data are reported in the upper bar diagram. Each DPV curve in the lower part corresponds to an upper bar.

current decrease resulted when specific binding occurred between the biotin probe and the target RNA (curve f).

The interfacial modification of the electrode before and after peptide attachment has been confirmed using FTIR based on the appearance of new characteristic peaks (Figure 2A). In our results, the peaks at 1565 and 1496 cm^{-1} in the PANI nanowire-coated substrate (curve a) can be assigned to the C=C stretching vibrations of the quinoid ring and benzenoid ring, separately. A narrow peak appeared at a frequency of 1243 cm^{-1} owing to the stretching and bending of the C–C bond. The bands at 1302 and 1146 cm^{-1} corresponded to various stretching connected with the C–N bond of secondary aromatic amine, and a C–H out-of-plane bending band appeared at 803 cm^{-1} . These characteristic peaks were consistent with previous reports about PANI.^{35,36} The spectrum of the peptide-modified electrode (curve b) also showed five distinctive peaks at 1572, 1476, 1296, 1245, and 811 cm^{-1} . An additional peak in the region of 1690–1630 cm^{-1} appeared at 1645 cm^{-1} , which is a characteristic of the formed amides.^{37–39} This indicates that the designed peptides were successfully fixed onto the PANI film.

To further confirm the surface changes, XPS spectra were recorded after PANI modification, biotin peptide immobilization, and biotin probe attachment (Figure 2B–D). All XPS survey spectra displayed Cl, C, N, and O peaks for PANI nanowire-coated electrodes. C_{1s} and N_{1s} peaks could be assigned to the PANI film, and a Cl_{2p} peak was seen due to HClO_4 doping during electrodeposition.

After incubation in biotin peptides, the Cl_{2p} peak decreased together with the appearance of two obvious S peaks (S_{2s} and S_{2p}) at 164 and 228 eV, which can be assigned to the cysteine and biotin of the peptide, indicating its successful immobilization. Following the SA and biotin probe assembly, a new P_{2s} peak emerged due to the phosphate skeleton from the probe. All characterization results are consistent with the previously discussed electrochemical measurements and provide confirmation of the successful assembly of the biosensor.

Optimization of Experimental Conditions. Only under optimal experimental conditions, the constructed biosensor would give the best sensing performance. Hence, we investigated the influence of the incubation time of the SA, concentration and immobilization time of the biotin probe, and hybridization time of the target N-gene, as depicted in Figure S4. Based on this study, the following optimized conditions were selected and employed for the analytical sensing operations: (A) SA incubation time, 60 min; (B) biotin probe immobilization time, 90 min; (C) biotin probe concentration, 2 μM ; and (D) target N-gene hybridization time, 60 min.

Antifouling Performance. To study the antifouling performance of the newly designed inverted Y-shaped peptide, bare and PANI- and biotin-peptide/PANI-coated GCEs were immersed in different single proteins and complex biological suspension liquids, and then, current changes [signal suppression = $(\Delta I/I_0) \times 100\%$, $\Delta I = I_0 - I$, I_0 and I represent the peak current of DPV before and after immersion in interference solutions for 30 min, respectively] caused by non-specific adsorption of interferences were recorded. As displayed in Figure 3A–C, the current-changing trends for different interfaces were similar after the incubation in the solution of negatively charged BSA, neutral Mb, and positively charged Lys with increasing signal suppression at higher protein concentrations. However, the current variation of the

biotin-peptide/PANI/GCE (red bar) was significantly smaller than that of the bare GCE (orange bar) and PANI (blue bar)-modified electrode, revealing the excellent resistance to single-protein adsorption by the electrode modified with the peptide. Knowing that proteins generally tend to adsorb onto hydrophobic interfaces rather than on hydrophilic ones,⁷ these results also demonstrated the good hydrophilicity of the peptides, consistent with the water contact angle results. Following, human serum was chosen to be the complex biological sample to test the antifouling performance, and the influence of the biotin probe and SA on antifouling performance was also investigated, as shown in Figure 3D–F. The lower parts were the original DPV data and the upper parts represent statistical analyses after being incubated in various concentrations of human serum of the bare GCE, PANI/GCE, and biotin-probe/SA/biotin-peptide/PANI/GCE. Again, the superior antifouling performance of the biotin-probe/SA/biotin-peptide/PANI/GCE over the other two interfaces can be noticed, although the non-antifouling biotin probe and SA were introduced into the interfaces. This result may be ascribed to the adequate coverage by peptide coating and the excellent antifouling ability of the newly designed inverted Y-shaped peptide. Remarkably, even after soaking in 20% human serum, the signal suppression by the peptide-modified electrode was 4.92%, indicating promising potential for real application.

In order to describe the antifouling characteristics more intuitively, the bare and PANI- and biotin-peptide/PANI-modified electrodes were incubated in PBS buffer (10 mM, pH 7.4) containing 0.2 $\text{mg}\cdot\text{mL}^{-1}$ FITC-BSA for 2 h to allow protein adsorption, and then, the protein adsorption behaviors at different interfaces were analyzed using fluorescence microscopy, as summarized in Figures 4A and S5. The amount of protein adsorption is reflected by fluorescence intensity. The bare GCE showed the strongest fluorescent (first column), followed by the PANI/GCE surface (second column), while the biotin-peptide/PANI/GCE (third column) showed the weakest fluorescent intensity. Similarly, confocal fluorescent images were shown in Figures 4A and S6 after incubation in Cy5-DNA solution for 2 h. The biotin-peptide/PANI-modified GCE exhibited good resistance to DNA adsorption. Based on all the results mentioned above, it can be concluded that the newly designed inverted Y-shaped peptide possesses excellent and stable antifouling properties toward single proteins and even concentrated complex biological media. Long-term antifouling performance was also investigated, as displayed in Figure S7. Additionally, a comparison antifouling experiment was carried out between the newly designed branched peptide and a linear peptide (control peptide) in different concentrations of FBS. As shown in Figure 4B, the newly designed inverted Y-shaped peptide displayed better antifouling performance compared to the control peptide at every used concentration. These results could be due to both the good water permeability of the film, which helps in improving the hydrophilicity^{40,41} and also the improved interface coverage by the antifouling anchor side chains.

Electrochemical Detection of the COVID-19 N-Gene.

After incubation in a series of concentrations of the target N-gene, the DPV measurements were performed to record the current change caused by the hybridization between the biotin probe and the target RNA, for the quantitative detection of the target N-gene (Figure 5A). As depicted in Figure 5B, the result showed a good linear relation between the logarithm of the

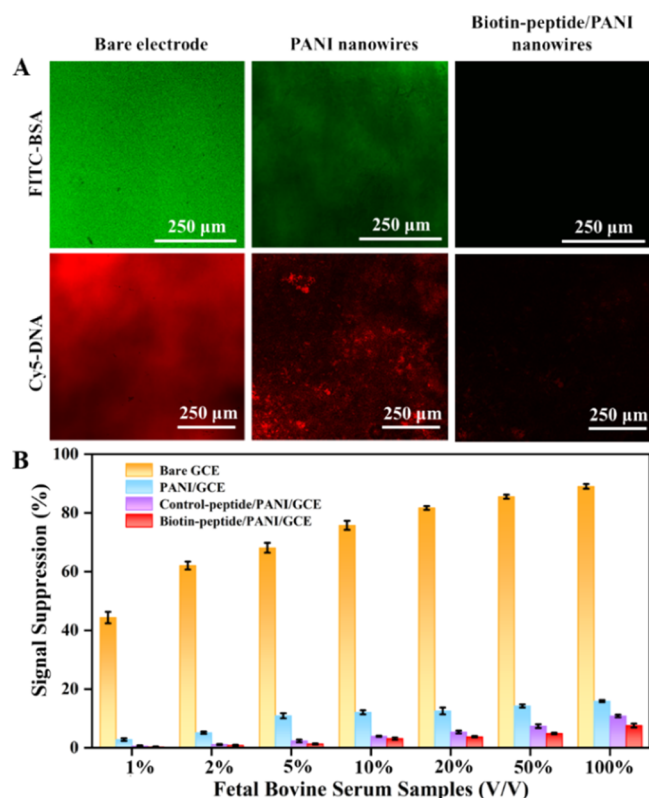


Figure 4. (A) Antifouling performances of the bare (first column), PANI nanowire-modified (second column), biotin-peptide/PANI nanowire (third column)-modified GCE against FITC-BSA and Cy5-DNA (2 h incubation) monitored by fluorescence microscopy. (B) Comparative antifouling performance of the bare and PANI-, control-peptide/PANI-, and biotin-peptide/PANI-modified GCE in FBS samples (V/V). Control-peptide (linear), CKEKEKEKE-KEPPPPKEKEKEKEK-biotin; biotin-peptide, (CKEKEKEKE)₂KEPPPPKEKEKEKEK-biotin.

target concentration (10^{-14} to 10^{-9} mol·L⁻¹) and the current signal under the optimal conditions. The linear fitting equation is ΔI (μ A) = 4.89 log C + 71.88, and the limit of detection (LOD) was calculated as 3.5 fM ($S/N = 3$). In addition, when the same experiment was performed in target solution containing 10% FBS, the linear regression equation is ΔI (μ A) = 5.28 log C + 77.23, which was similar to that in pure

target solution (Figure 5C). This means that the electrode interface was almost not affected by the presence of interferences in the FBS. Furthermore, the preliminary application in human serum was also investigated by a standard addition method with acceptable recoveries from 98.03% to 101.63% (Table S2), indicating that the developed biosensor has great potential for practical application. Such remarkable performance can be attributed to the excellent electrochemical properties of the PANI conducting polymer being used as an interface substrate, which provided a sensitive current signal, and to the good antifouling properties of the newly designed peptide that effectively resists interferences even in complex matrix systems. Given that there are few reports on the detection of COVID-19 by electrochemical methods, Table S3 lists the performance of several different approaches for the detecting COVID-19.

Stability, Selectivity, and Reproducibility of the Genosensor. Stability, selectivity, and reproducibility represent three important parameters to be verified for biosensor systems. The stability of the genosensor here fabricated (biotin-probe/SA/biotin-peptide/PANI/GCE) was first studied by consecutive CV tests in 0.2 M PBS (pH 7.4) for 50 cycles. As displayed in Figure S8A, the genosensor exhibited outstanding stability with almost unchanged peak current and potential after 50 cycles scan. Furthermore, the stability of the prepared genosensor was also monitored by interval tests within 10 days, with the signal retention of 92.8% and relative standard deviations (RSD) of 1.51% (Figure S8B). The selectivity of the genosensor was tested with 10^{-9} M miRNA-21 and miRNA-141, noncomplementary, as interferences. Even when the concentration of interfering agents was about 100 times larger than that of the target, no obvious responses were observed from current signals and the current variation value of the genosensor toward the mixture showed almost equal to that of the target, demonstrating the good selectivity of the genosensor (Figure S9). To further explore the reproducibility, we used the same biosensor to detect two concentrations (low and high), 10 fM and 1 nM target COVID-19 N-gene. The RSDs were 3.06% and 1.62% (Figure S10), respectively, showing good accuracy and reproducibility.

CONCLUSIONS

Overall, a sensitive and robust electrochemical genosensor was fabricated employing a newly designed peptide as an

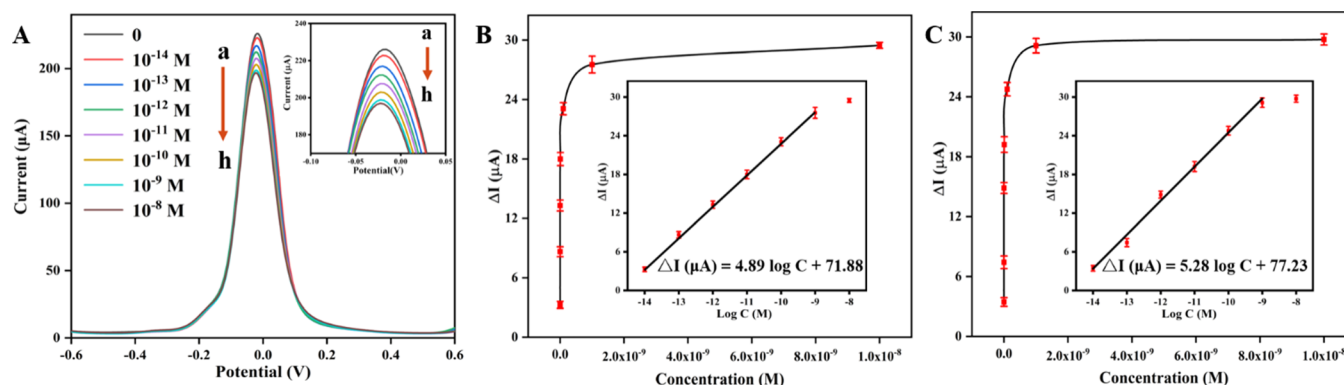


Figure 5. (A) DPV responses of the genosensor after incubation in different concentrations of target N-gene solutions, curves from a to h: 10^{-14} to 10^{-8} M. Inset: partial enlargement of the current peaks. Current response of the genosensor for the COVID-19 N-gene in PBS (0.2 M, pH 7.4) (B) and complex biological media (10% FBS) (C). The inset shows the corresponding calibration curves. Error bars represent the standard deviations of the three measurements.

antifouling agent integrated into a PANI nanowire platform for the COVID-19 N-gene. This electrochemical system exhibited extraordinary antifouling properties thanks to the designed inverted Y-shaped peptide with two anchoring branches, which bind tightly to the surface of PANI nanowires and effectively resist the nonspecific adsorption. PANI nanowires not only provided a large surface area for the immobilization of biomolecules but also enabled sensitive current signal generation. The fabricated genosensor demonstrated exceptional antifouling properties in parallel with remarkable analytical ability for the COVID-19 N-gene, reaching LOD as low as 3.5 fM even in complex human serum samples and exhibiting promising potential for early detection of COVID-19 viral infection in decentralized settings.

■ ASSOCIATED CONTENT

SI Supporting Information

The Supporting Information is available free of charge at <https://pubs.acs.org/doi/10.1021/acs.analchem.1c00724>.

Investigation of the newly designed inverted Y-shaped peptide; optimization of the experimental conditions; antifouling ability of different surfaces in FITC-BSA and Cy5-DNA; long-term antifouling performance; stability of the genosensor; selectivity of the genosensor; reproducibility of the genosensor; water contact angle of different modified electrodes; preliminary application of the genosensor; and performance comparison of different approaches (PDF)

■ AUTHOR INFORMATION

Corresponding Authors

Caifeng Ding – Key Laboratory of Optic-Electric Sensing and Analytical Chemistry for Life Science, MOE, Shandong Key Laboratory of Biochemical Analysis, Key Laboratory of Analytical Chemistry for Life Science in Universities of Shandong, College of Chemistry and Molecular Engineering, Qingdao University of Science and Technology, Qingdao 266042, PR China; orcid.org/0000-0002-5281-0158; Phone: +86 53284022990; Email: caifengding@qust.edu.cn; Fax: +8653284022681

Xiliang Luo – Key Laboratory of Optic-Electric Sensing and Analytical Chemistry for Life Science, MOE, Shandong Key Laboratory of Biochemical Analysis, Key Laboratory of Analytical Chemistry for Life Science in Universities of Shandong, College of Chemistry and Molecular Engineering, Qingdao University of Science and Technology, Qingdao 266042, PR China; orcid.org/0000-0001-6075-7089; Email: xiliangluo@qust.edu.cn

Authors

Zhen Song – Key Laboratory of Optic-Electric Sensing and Analytical Chemistry for Life Science, MOE, Shandong Key Laboratory of Biochemical Analysis, Key Laboratory of Analytical Chemistry for Life Science in Universities of Shandong, College of Chemistry and Molecular Engineering, Qingdao University of Science and Technology, Qingdao 266042, PR China

Yihui Ma – Key Laboratory of Optic-Electric Sensing and Analytical Chemistry for Life Science, MOE, Shandong Key Laboratory of Biochemical Analysis, Key Laboratory of Analytical Chemistry for Life Science in Universities of Shandong, College of Chemistry and Molecular Engineering,

Qingdao University of Science and Technology, Qingdao 266042, PR China

Min Chen – Key Laboratory of Optic-Electric Sensing and Analytical Chemistry for Life Science, MOE, Shandong Key Laboratory of Biochemical Analysis, Key Laboratory of Analytical Chemistry for Life Science in Universities of Shandong, College of Chemistry and Molecular Engineering, Qingdao University of Science and Technology, Qingdao 266042, PR China

Adriano Ambrosi – Key Laboratory of Optic-Electric Sensing and Analytical Chemistry for Life Science, MOE, Shandong Key Laboratory of Biochemical Analysis, Key Laboratory of Analytical Chemistry for Life Science in Universities of Shandong, College of Chemistry and Molecular Engineering, Qingdao University of Science and Technology, Qingdao 266042, PR China; orcid.org/0000-0002-0581-4658

Complete contact information is available at:

<https://pubs.acs.org/doi/10.1021/acs.analchem.1c00724>

Author Contributions

†Z.S. and Y.M. contributed equally.

Notes

The authors declare no competing financial interest.

■ ACKNOWLEDGMENTS

This work is supported by the National Natural Science Foundation of China (21974075 and 21675093), the Double-Hundred Program for Foreign Experts of Shandong Province (WST2019011), and the Taishan Scholar Program of Shandong Province of China (ts20110829).

■ REFERENCES

- (1) Seo, G.; Lee, G.; Kim, M. J.; Baek, S.-H.; Choi, M.; Ku, K. B.; Lee, C.-S.; Jun, S.; Park, D.; Kim, H. G.; Kim, S.-J.; Lee, J.-O.; Kim, B. T.; Park, E. C.; Kim, S. I. *ACS Nano* **2020**, *14*, 5135–5142.
- (2) WHO. *Coronavirus Disease 2019 (COVID-19): Situation Report* <https://www.who.int/publications/m/item/weekly-operational-update-on-covid-19--8-february-2021>.
- (3) Carter, L. J.; Garner, L. V.; Smoot, J. W.; Li, Y.; Zhou, Q.; Saveson, C. J.; Sasso, J. M.; Gregg, A. C.; Soares, D. J.; Beskid, T. R.; Jervey, S. R.; Liu, C. *ACS Cent. Sci.* **2020**, *6*, 591–605.
- (4) Yu, L.; Wu, S.; Hao, X.; Dong, X.; Mao, L.; Pelechano, V.; Chen, W.-H.; Yin, X. *Clin. Chem.* **2020**, *66*, 975–977.
- (5) Lim, R. R. X.; Bonanni, A. *TrAC, Trends Anal. Chem.* **2020**, *133*, 116081.
- (6) Udugama, B.; Kadhiresan, P.; Kozłowski, H. N.; Malekjahani, A.; Osborne, M.; Li, V. Y. C.; Chen, H.; Mubareka, S.; Gubbay, J. B.; Chan, W. C. W. *ACS Nano* **2020**, *14*, 3822–3835.
- (7) Kim, H. *Eur. Radiol.* **2020**, *30*, 3266–3267.
- (8) Wang, W.; Xu, Y.; Gao, R.; Lu, R.; Han, K.; Wu, G.; Tan, W. *JAMA, J. Am. Med. Assoc.* **2020**, *323*, 1843–1844.
- (9) Song, Z.; Chen, M.; Ding, C.; Luo, X. *Anal. Chem.* **2020**, *92*, 5795–5802.
- (10) Wang, J.; Xu, G.; Wang, W.; Xu, S.; Luo, X. *Chem. - Asian J.* **2015**, *10*, 1892–1897.
- (11) Wang, G.; Han, R.; Li, Q.; Han, Y.; Luo, X. *Anal. Chem.* **2020**, *92*, 7186–7193.
- (12) Gooding, J. J. *Nat. Nanotechnol.* **2019**, *14*, 1089–1090.
- (13) Nir, S.; Zanuy, D.; Zada, T.; Agazani, O.; Aleman, C.; Shalev, D. E.; Reches, M. *Nanoscale* **2019**, *11*, 8752–8759.
- (14) Song, Z.; Li, Y.; Teng, H.; Ding, C.; Xu, G.; Luo, X. *Sens. Actuators, B* **2020**, *305*, 127329.
- (15) Ding, C.; Wang, X.; Luo, X. *Anal. Chem.* **2019**, *91*, 15846–15852.

- (16) Liu, B.; Liu, X.; Shi, S.; Huang, R.; Su, R.; Qi, W.; He, Z. *Acta Biomater.* **2016**, *40*, 100–118.
- (17) Nowinski, A. K.; Sun, F.; White, A. D.; Keefe, A. J.; Jiang, S. J. *Am. Chem. Soc.* **2012**, *134*, 6000–6005.
- (18) Arul, A.; Sivagnanam, S.; Dey, A.; Mukherjee, O.; Ghosh, S.; Das, P. *RSC Adv.* **2020**, *10*, 13420–13429.
- (19) Liu, N.; Song, J.; Lu, Y.; Davis, J. J.; Gao, F.; Luo, X. *Anal. Chem.* **2019**, *91*, 8334–8340.
- (20) Rao, H.; Chen, M.; Ge, H.; Lu, Z.; Liu, X.; Zou, P.; Wang, X.; He, H.; Zeng, X.; Wang, Y. *Biosens. Bioelectron.* **2017**, *87*, 1029–1035.
- (21) Yang, L.; Yang, L.; Wu, S.; Wei, F.; Hu, Y.; Xu, X.; Zhang, L.; Sun, D. *Sens. Actuators, B* **2020**, *323*, 128689.
- (22) Liu, X.; Wang, Y.; Zhu, L.; Tang, Y.; Gao, X.; Tang, L.; Li, X.; Li, J. *Sens. Actuators, B* **2020**, *323*, 128694.
- (23) Saha, A.; Nir, S.; Reches, M. *Langmuir* **2020**, *36*, 4201–4206.
- (24) Xia, N.; Sun, Z.; Ding, F.; Wang, Y.; Sun, W.; Liu, L. *ACS Sens.* **2021**, *6*, 1166–1173, DOI: 10.1021/acssensors.0c02415.
- (25) La, M.; Wu, D.; Gao, Y.; Xia, N.; Niu, Y.; Liu, L.; Yi, X. *Electrochem. Commun.* **2020**, *118*, 106791.
- (26) Fang, X.; Jiang, W.; Han, X.; Zhang, Y. *Microchim. Acta* **2013**, *180*, 1271–1277.
- (27) Meng, X.; Xu, M.; Zhu, J.; Yin, H.; Ai, S. *Electrochim. Acta* **2012**, *71*, 233–238.
- (28) Wang, G.; Han, R.; Su, X.; Li, Y.; Xu, G.; Luo, X. *Biosens. Bioelectron.* **2017**, *92*, 396–401.
- (29) Song, Z.; Sheng, G.; Cui, Y.; Li, M.; Song, Z.; Ding, C.; Luo, X. *Microchim. Acta* **2019**, *186*, 220.
- (30) Xie, S.; Dong, Y.; Yuan, Y.; Chai, Y.; Yuan, R. *Anal. Chem.* **2016**, *88*, 5218–5224.
- (31) He, Y.; Jiao, B. *Sens. Actuators, B* **2018**, *265*, 387–393.
- (32) Xia, Y.; Adibnia, V.; Huang, R.; Murschel, F.; Faivre, J.; Xie, G.; Olszewski, M.; De Crescenzo, G.; Qi, W.; He, Z.; Su, R.; Matyjaszewski, K.; Banquy, X. *Angew. Chem., Int. Ed.* **2019**, *58*, 1308–1314.
- (33) Molino, P. J.; Yang, D.; Penna, M.; Miyazawa, K.; Knowles, B. R.; MacLaughlin, S.; Fukuma, T.; Yarovsky, I.; Higgins, M. J. *ACS Nano* **2018**, *12*, 11610–11624.
- (34) Liu, N.; Hui, N.; Davis, J. J.; Luo, X. *ACS Sens.* **2018**, *3*, 1210–1216.
- (35) Guo, Q.; Yi, C.; Zhu, L.; Yang, Q.; Xie, Y. *Polymer* **2005**, *46*, 3185–3189.
- (36) Zhao, M.; Wu, X.; Cai, C. *J. Phys. Chem. C* **2009**, *113*, 4987–4996.
- (37) Hui, N.; Sun, X.; Niu, S.; Luo, X. *ACS Appl. Mater. Interfaces* **2017**, *9*, 2914–2923.
- (38) Ye, H.; Wang, L.; Huang, R.; Su, R.; Liu, B.; Qi, W.; He, Z. *ACS Appl. Mater. Interfaces* **2015**, *7*, 22448–22457.
- (39) Matharu, Z.; Sumana, G.; Arya, S. K.; Singh, S. P.; Gupta, V.; Malhotra, B. D. *Langmuir* **2007**, *23*, 13188–13192.
- (40) Choudhury, R. R.; Gohil, J. M.; Mohanty, S.; Nayak, S. K. *J. Mater. Chem. A* **2018**, *6*, 313–333.
- (41) Liu, Z.; An, X.; Dong, C.; Zheng, S.; Mi, B.; Hu, Y. *J. Mater. Chem. A* **2017**, *5*, 23190–23197.